Journal of
Marine Science and Engineering

MDPI

Article

Small-Scale Renewable Energy Converters for Battery Charging

Mohd Nasir Ayob [1,2,*], Valeria Castellucci [1], Malin Göteman [1], Joakim Widén [3], Johan Abrahamsson [1], Jens Engström [1] and Rafael Waters [1]

1 Swedish Centre for Renewable Electric Energy Conversion, Division for Electricity, Department of Engineering Sciences, The Ångstrom Laboratory, P.O Box 534, SE-75121 Uppsala, Sweden; Valeria.Castellucci@angstrom.uu.se (V.C.); Malin.Goteman@angstrom.uu.se (M.G.); Johan.Abrahamsson@angstrom.uu.se (J.A.); Jens.Engstrom@angstrom.uu.se (J.E.); Rafael.Waters@angstrom.uu.se (R.W.)
2 School of Mechatronic Engineering, Universiti Malaysia Perlis, 02600 Arau, Perlis, Malaysia
3 Built Environment Energy Systems Group (BEESG), Division of Solid State Physics, Department of Engineering Sciences, Uppsala University, PO Box 534, 751 21 Uppsala, Sweden; Joakim.Widen@angstrom.uu.se
* Correspondence: Nasir.Ayob@angstrom.uu.se; Tel.: +46-18-471-5849

Received: 14 January 2018; Accepted: 5 March 2018; Published: 13 March 2018

Abstract: This paper presents two wave energy concepts for small-scale electricity generation. In the presented case, these concepts are installed on the buoy of a heaving, point-absorbing wave energy converter (WEC) for large scale electricity production. In the studied WEC, developed by Uppsala University, small-scale electricity generation in the buoy is needed to power a tidal compensating system designed to increase the performance of the WEC in areas with high tides. The two considered and modeled concepts are an oscillating water column (OWC) and a heaving point absorber. The results indicate that the OWC is too small for the task and does not produce enough energy. On the other hand, the results show that a hybrid system composed of a small heaving point absorber combined with a solar energy system would be able to provide a requested minimum power of around 37.7 W on average year around. The WEC and solar panel complement each other, as the WEC produces enough energy by itself during wintertime (but not in the summer), while the solar panel produces enough energy in the summer (but not in the winter).

Keywords: small wave energy converter; oscillating water column; heaving point absorber

1. Introduction

The working principle of the wave energy converter (WEC) from Uppsala University is a heaving point absorber [1–3]. The buoy motion in the heave direction is converted to linear motion in the translator inside a linear generator [4,5]. Several techniques have been implemented in order to optimize the power absorption, e.g., [1,6,7]. In areas of high tide, the length of the buoy line needs to be continually changed in order to optimize energy conversion, and a tidal compensator has been designed to this end. A prototype of a tidal compensator, suitable for the Swedish west coast, has been developed to compensate for tidal variations of up to 1 m [8].

This paper discusses the next-generation compensator system from Uppsala University [9]. The main difference from the previous system is that the present compensator range is as large as 8 m, dimensioned for the wave climate at the Wave Hub, of the southwest coast of England. Wave Hub, located off the west coast of Cornwall, is the one of the world's largest sites for renewable energy technology testing and development [10]. Wave Hub offers modern offshore and onshore infrastructure for WEC deployment with available facilities including subsea cable connection, an onshore substation,

and grid connection. The authors of [11] present the wave resource assessment at the Wave Hub characterized by an average significant wave height and energy period of 2 m and 7 s, respectively. A peak-to-peak variation of the tidal level at the Newlyn Tidal Observatory, 22 km south of Wave Hub, was registered at 6.6 m [12]. The effect of tidal variation to certain types of WECs at the Wave Hub research site has been studied by Castellucci et al. [13]. The main part of the tidal compensator is a winch that releases and retracts a steel chain connecting the buoy to the buoy line [9]. The system is powered by two 12 V batteries. From the experiences gained with the previous tidal compensator, the system needs a reliable power source to charge the batteries [14]. To meet this challenge, a number of renewable energy converters (RECs) have been considered, and these converters need to fulfill a number of criteria: The energy converters must be small enough to be attached to the main buoy of the WEC while the buoy's operation is undisturbed. Furthermore, the structure must also be strong enough to survive the harsh sea environment. Because of the exposure of a buoy-mounted wind turbine to overtopping waves, the structure is not considered to be a mechanically viable system, and the power from a small wind turbine is therefore not considered suitable. The current analysis is therefore focused on extracting the energy from ocean waves and/or solar. The idea of harvesting wave energy for a self-powered device is not new. Yoshio Masuda was the first to develop a wave energy converter for a self-powered navigation buoy [15]. Recently, utilizing the same method of wave energy conversion, Henriques et al. [16] optimized an oscillating water column (OWC)-type WEC for self-powered sensor buoys. Another example is given in [17], where a dielectric elastomer is used to harness wave energy from a wide range of wave frequencies.

The paper is organized as follows. Section 2 describes the energy required to operate the tidal compensator and to charge the battery in standby mode as well as in operating mode. Section 3 describes the estimated power production from an OWC-type WEC and from a heaving, point-absorbing WEC. The results and discussion are presented in Section 4. The conclusion is presented in Section 5.

2. Energy Required by the Compensator System

A compensator system driven by a DC motor has previously been developed at Uppsala University [9]. A reliable power source is important for operating the compensator system but to acquire this energy from the main WEC is technically challenging and not considered feasible at this point in development. Moreover, to obtain power from a marine substation (on the seabed far away from the main WEC) up to the buoy on the surface is also not a practical solution. This leaves the option of producing the energy directly at the point absorbing buoy, which is the focus of this study.

A DC motor with a rated power of 1.5 kW is used to drive the system. The gearbox used in the system is of a planetary type with five reductions and a gear ratio of 4758 manufactured by Bonfiglioli [18], see Figure 1. The dynamic efficiency of the gearbox is 0.85. One important difference from the previous concept described in [8,14] is that it does not have to overcome the forces that come from the self-locking mechanism. Therefore, the energy required to increase the length of the buoy line is minimal as the 10-ton weight of the buoy line and the translator will be sufficient to turn the winch. The position and speed control during the downward motion is determined by the application of an electromagnetic-release spring-applied brake from INTORQ GmbH & Co [19]. The brake is always in the braking position unless the electromagnet is powered with 19 W, which works to release the brake. In the operating mode, the power from the batteries is thus needed for both turning the motor and releasing the brake. The system is set to start adjusting the connection line when the sea level variation exceeds 0.1 m.

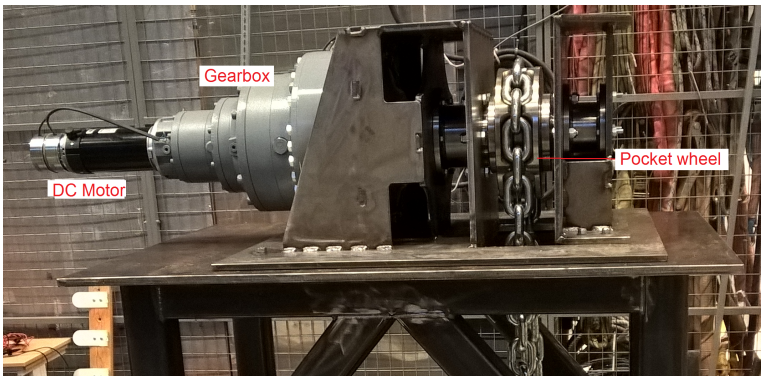

Figure 1. The winch system consists of a gearbox, a DC motor, a steel chain, and a pocket wheel. The pitch diameter of the pocket wheel is 0.32 m.

To estimate the system's power consumption, two modes have been considered: standby mode and operating mode. The power in standby mode is 5–8 W. These power levels are based on the expected improvements on the previous system in [14]. The energy for the DC motor was estimated after the dynamic efficiency of the gearbox and the losses in the DC motor were considered. The motor is intended to rotate at an operating speed of 1500 rpm. This rotational speed, converted to the linear speed of translator-retract/release is around 0.32 m/min. Table 1 summarizes the estimated energy required by the compensator to reach the maximum designated range of 8 m.

Table 1. Average energy required by the compensator over a 24 h period (every semi-diurnal cycle).

Compensator Operation	Standby Mode	Operating Mode (Wh)		Total Energy/Day
	(Communication + Control)	Release Brake	Motor	(Wh/Day)
Releases (2 × 6 h)	8 W × 12 h	19 W × 2 × 52 s	-	96.6
Retracts (2 × 6 h)	8 W × 12 h	19 W × 2 × 0.48 h	723.2 W × 2 × 0.48 h	808.5

Based on the total energy consumption of 905.1 Wh/day, which is the sum of values in the last column of Table 1, the average power needed to charge the batteries is approximately 37.7 W. A suitable battery charging mechanism is thus needed with the capability of providing at least 37.7 W to the considered 100 Ah, two 12 V battery system. The limitation in the design of a small REC to accomplish this task is the limited space (as the REC would be mounted to the large WEC buoy) and that the REC should be able to operate and survive in the harsh ocean environment.

Solar panels are known to be robust and are easily available commercially. Four CT50 SolarMarine [20] solar panels units with a nominal voltage of 12 V and a power of 50 W will each provide a total peak power of 200 W. However, the usual limitations on the performance of the solar panels apply. They will be able to provide peak power during the summer season, but during the winter season the energy output from the solar panels is insufficient. It is not enough to rely on solar panels to charge the batteries; thus, in this case, energy from the waves are considered in a hybrid system.

3. Method

3.1. Sea State and Solar Irradiation at Wave Hub

The most commonly occurring sea state at Wave Hub is characterized by a significant wave height, Hs, of 1.25 m and a wave energy period, Te, of 5.25 s, see Figure 11 in [11]. We define this sea state as Wave1 in this paper. Considering that the power from solar photovoltaics (PV) would be minimal in the winter season (see Figure 2), a typical wave characteristic from a winter month (e.g., December 2015) at the Wave Hub [21] was also considered for the analysis. Here, we define this as Wave2. Wave2 is

characterized by Hs = 3.75 m and Te = 7.32 s. These parameters were used in Bretschneider spectra [22] to generate a time series of the incident waves, y. The solar irradiation information and the analysis of contribution from solar PVs was obtained from a Photovoltaic Geographical Information System (PVGIS) [23]. The calculation of the performance is based on hourly values of irradiation in a given location (in this case, Lat: 50.3476 and Lon: −5.6129) over a period of five years (2007–2011). Figure 2 shows a monthly solar irradiation (horizontal) at Wave Hub obtained from PVGIS.

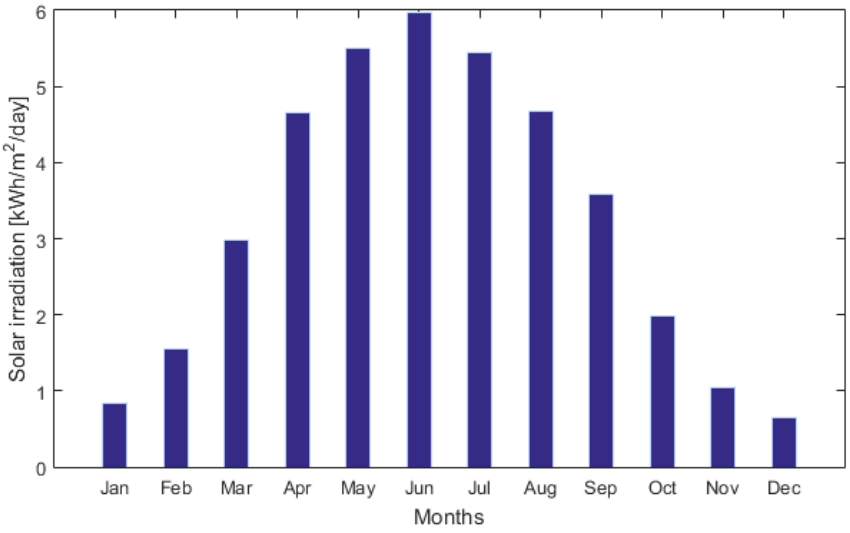

Figure 2. Monthly solar irradiation (horizontal) at Wave Hub obtained from PVGIS [23].

3.2. Power from an OWC

The OWC can be considered as one of the simplest WEC concepts. The first large scale onshore prototype was developed at the end of the 1980's. Efforts have been made to improve the efficiency and operating performance of OWCs by Sarmento [24], Evans and Porter [25], Morris-Thomas et al. [26] and Ram [27]. Dynamic modeling and experimental verification of small-scale OWC WECs have been studied by Bayoumi [28]. Because of its simplicity, a small OWC is considered as a potential power source for the battery system and tidal compensator.

As shown in Figure 3, the small OWC is installed in a buoy with an air chamber and air-driven turbine and generator as the PTO. A cylindrical buoy with a small chamber at the center of the buoy was used in the simulation to simplify the analysis. However, in practice, the position of the air chamber would be a bit off from the center of the buoy to give space to the buoy line. As the size of the chamber is small (a 0.4 m diameter) compared to the buoy (a 6 m diameter), the position of the chamber in the real case would not lead to a big difference in the water level in the chamber in the simulations. Figure 4 shows the result of the surface elevation in the chamber from simulations in WAMIT® with the parameters listed in Table 2. The interaction between the ocean waves, $y(t)$, and the buoy introduces a motion in the vertical direction, h, of the water surface in the air chamber. This motion creates a relative motion , d between h and s, and acts as the driving force for the OWC. At equilibrium $h = s = d = 0$. Assuming that the water surface in the air chamber is flat, due to the large wavelength compared to the chamber's diameter, the water surface inside the chamber acts as a piston with the vertical position d. This water piston moves up and down, compressing and expanding the air in the chamber and simultaneously forcing air through the turbine.

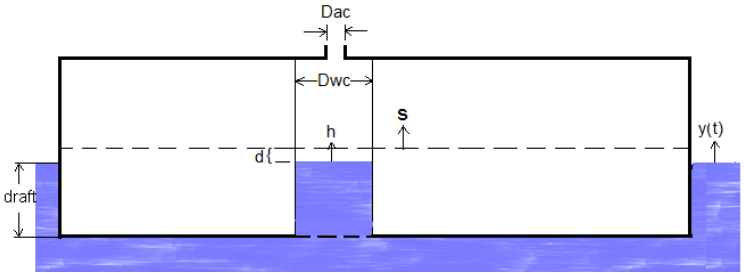

Figure 3. Cross-sectional view of a cylindrical buoy. The OWC consists of an air chamber with diameter Dwc and an air turbine placed in the outlet with diameter Dac. $y(t)$, s, and h are the water surface, the buoy position, and the water column position, respectively (not to scale).

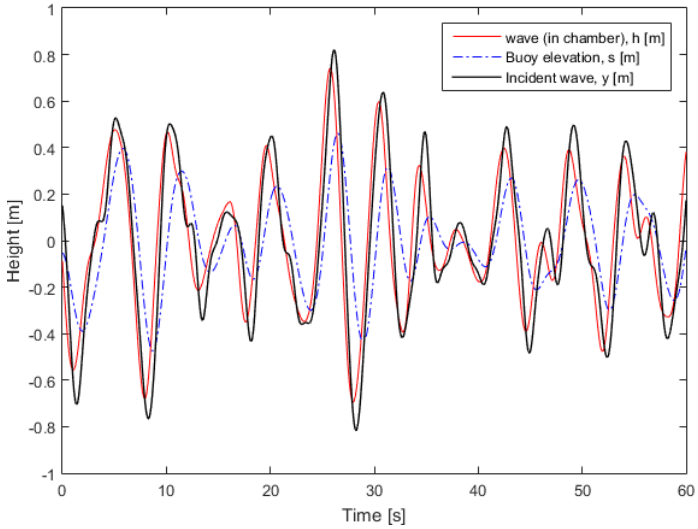

Figure 4. The simulation result from WAMIT showing the motion of the wave in the chamber, the buoy, and the incident wave. The incident wave, y, is the most commonly occurring sea state (Wave1) in the region of study.

Table 2. The oscillating water column (OWC) model dimensions.

Parameter	Dimension
Buoy radius	3.0 m
Buoy weight	5736 kg
Water column diameter, Dwc	0.40 m
Turbine tube diameter, Dac	0.06 m
Buoy draft	0.42 m

A control volume [29] can be used to estimate the maximum power that the OWC system can absorb (i.e., limited space and relatively small wave height). The air in the chamber is considered the control volume $V_a(t)$. A mass balance equation is used to obtain the velocity of air going in and out of the air chamber through the turbine. Referring to Figure 3, the volume of air in the chamber at any time t is given as

$$V_a(t) = V_c - V_w(t) = V_c - \iint y(t)\,\mathrm{d}A = V_c - A\int \mathrm{d}d = V_c - Ad(t) \quad (1)$$

where V_c, V_w, A, and h are the chamber volume, the water volume inside the chamber, the piston area, and the piston elevation, respectively. The continuity equation for the control volume with mass for the air chamber, m_{cv} is given as

$$\dot{m}_{in} - \dot{m}_{out} = \frac{\mathrm{d}m_{cv}}{\mathrm{d}t} \tag{2}$$

where $\dot{m}_{in}$ and $\dot{m}_{out}$ are incoming and outgoing mass flow rates. By assuming that the fluid is incompressible, the rate of change of air volume, $\dot{V}_a(t)$, is equal to the air volume rate that passes the turbine

$$\dot{V}_a(t) = \frac{\mathrm{d}V(t)}{\mathrm{d}t} = \frac{-A\mathrm{d}d(t)}{\mathrm{d}t}. \tag{3}$$

From the Betz limit [30], the maximum rate of turbine extraction of kinetic energy from the moving air with speed v and mass flow rate $\dot{m}$ is $\frac{16}{27}$. Based on the above assumption, the instantaneous power from the system is determined by

$$\dot{E}_t = \frac{1}{2}\frac{16}{27}\dot{m}_a v^2 = \frac{8}{27}\frac{\rho_{air}\dot{V}_a(t)^3}{{A_c}^2} = \frac{-8\rho_{air}\dot{d}_a(t)^3 A^3}{27{A_c}^2} \tag{4}$$

where A_c is the tube cross section, and ρ_{air} the air density. The average energy output from the system for the time interval [0, T] with the generator efficiency is determined by η_{gen}

$$E_N = \int_0^T \eta_{gen}(t)\dot{E}_t(t)\,\mathrm{d}t. \tag{5}$$

3.3. Power from a Small Point Absorber WEC

Another option for a power source is a small, heaving, point-absorbing WEC. In this paper, we consider the motion of a small buoy (SB) connected to a generator, see Figure 5. The dimensions of the point absorber are similar to Figure 3 except that an SB is placed inside the chamber. Energy is extracted by damping the motion of the SB. Table 3 shows the SB parameters and a time series of wave elevation is shown in Figure 6a. The interaction between the ocean waves, $y(t)$, and the buoy, $s(t)$, introduces a wave motion in the chamber, $h(t)$, acting on the SB.

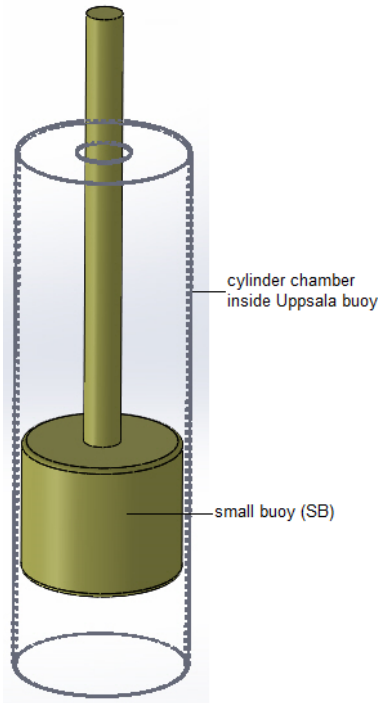

Figure 5. A small buoy is placed in a cylindrical chamber of the Uppsala buoy, see Figure 3.

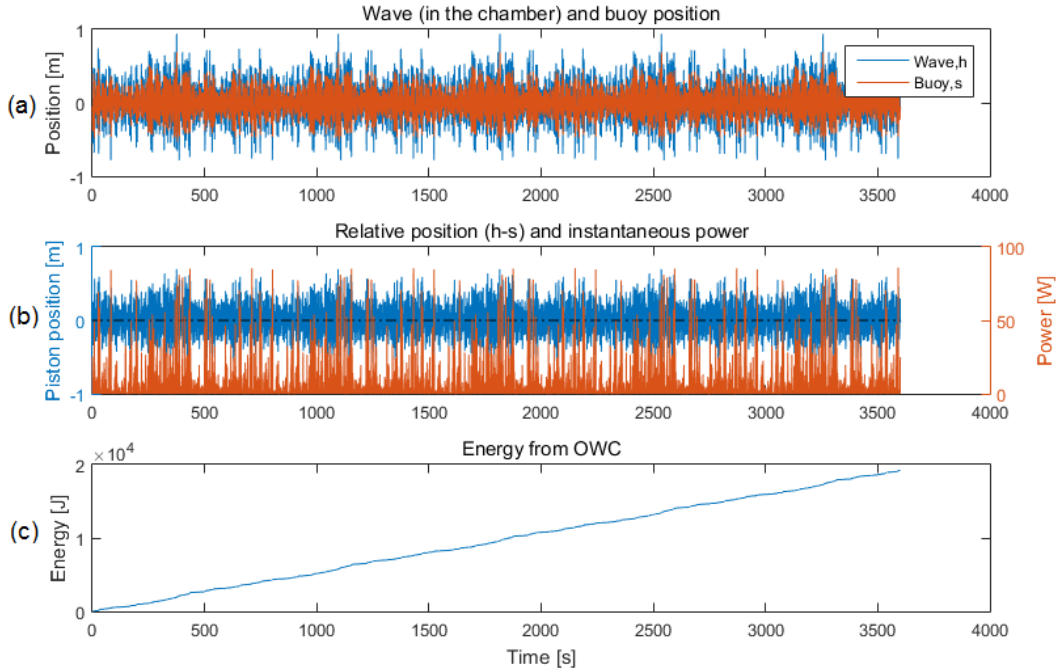

Figure 6. (**a**) The vertical position for the wave in the chamber and the buoy. (**b**) Instantaneous power and the relative position between the water surface in the OWC chamber and the buoy. (**c**) Cumulative energy production over 1 h.

Table 3. Parameters for the small buoy.

Parameter	Symbol	Dimension
Diameter SB	D	0.35 m
Total Mass SB	m	20 kg
Draft	-	0.20 m
Wave elevation	y	-
Buoy elevation	s	-
Wave (in chamber)	h	-
SB elevation	z	-

The general equation of motion for floating point-absorbing WECs is

$$\frac{md^2z}{dt^2} = F_e + F_r + F_h + F_{gen} \tag{6}$$

where m is the total mass of the small buoy and alternator, and F_{gen} is the damping force from the generator. F_e, F_r, and F_h are the excitation, radiation and hydrostatic force, respectively. The hydrodynamic forces are calculated by assuming linear potential flow theory [31]. The excitation force exerted on the SB is determined by a convolution of wave elevation $h(t)$ and the impulse response function of SB, $f_e(t)$

$$F_e(t) = f_e(t) * h(t). \tag{7}$$

The radiation force exerted on the SB is then defined as a convolution product of radiation impedance, $g(t)$ [7], with the SB's vertical velocity according to

$$F_r(t) = -g(t) * \dot{z}(t). \tag{8}$$

The buoyancy stiffness is proportional to the vertical elevation of the SB and is determined by

$$F_h = -\rho g A_{SB} z(t) \tag{9}$$

where ρ and z are the water density and the SB's vertical position respectively. The force from the generator counteracts the SB motion and is proportional to the velocity of the SB. The generator force with a damping coefficient γ is determined by

$$F_{gen} = -\gamma \dot{z}(t). \tag{10}$$

The total mass of the SB is set to 20 kg. The authors of [7] show how the system frequency can be shifted to coincide with the frequency of the incoming wave. By replacing Equations (7)–(10) into Equation (6) and performing Fourier transform into the frequency domain, the equations of motion take the form

$$(-\omega^2(m + m_a) + i\omega(\gamma + R) + \rho g A_{SB})\hat{z} = \hat{f}_e \hat{h}. \tag{11}$$

The hydrodynamics parameters f_e, R, and added mass,m_a for the SB were obtained from WAMIT®. The transfer function that relates the wave amplitude $\hat{h}$ with the SB elevation $\hat{z}$ is

$$\hat{H}(\omega) = \frac{\hat{f}_e}{-\omega^2(m + m_a) + i\omega(\gamma + R) + \rho g A_{SB}}. \tag{12}$$

The SB position z can be obtained by taking the convolution of the transfer function H with the wave amplitude h in the time domain and $z(t)$ is given by

$$z(t) = H(t) * h(t). \tag{13}$$

The stroke of the SB in vertical motion is limited to ± 0.5 m regardless of the amplitude of the incoming wave as the SB moves inside the big buoy. This can be realized in practice by placing two end-stop plates at the upper end and at the lower end of the SB path of motion. See [32] for details about end stop plates. The average power extracted from the wave by the PTO is given in Equation (10). In the time interval [0, t],

$$p(t) = \frac{1}{t} \int_0^t \gamma \, \dot{z}^2 \, \mathrm{d}t \tag{14}$$

4. Results and Discussion

4.1. The OWC

The plot in Figure 6a shows the wave elevation in the chamber and the WEC buoy responding to Wave1. The relative motion of the wave in the chamber and buoy, acting as the excitation force for the OWC, is shown in Figure 6b. Based on Equation (4), the instantaneous output power is calculated, see Figure 6b. Figure 6c shows the cumulative energy over 1 h and has an average power of 5.3 W. Based on Equation (4), the power output from the OWC is significantly influenced by the chamber diameter and the outlet diameter. The chamber diameter, *Dwc*, has been set to the maximum of 0.4 m because of the limited space in the buoy, and the tube diameter *Dac* is set to 0.06 m, which corresponds to a realistic size of the turbine. It should be noted that the results from the simulation are an ideal case with assumptions made to simplify the calculations. The air was assumed to be an incompressible fluid and the presence of turbine in the chamber outlet was not considered in the simulation. In reality, the vertical motion d will be smaller because of the reaction force from the air chamber acting in the opposite direction to the water piston as the energy is extracted by the turbine.

The kinetic energy conversion of air passing the turbine is also assumed at the maximum, i.e., the Betz limit. In reality, however, the actual value will be lower. Based on the ideal case of incompressible fluid, the conclusion made is that, by using an OWC (*Dwc* = 0.4 m and *Dac* = 0.06 m), the possible average-power at maximum absorption (5.3 W) is too low and far from sufficient to

provide power to the system. Moreover, in real cases, there will be even more energy losses because of the conversion efficiency and the non-ideal compressible fluid characteristics of air.

The technical details on the air turbine and its position in the chamber outlet were not discussed in this paper because of the above conclusion that the average power absorption is not sufficiently large for the intended application.

4.2. Heaving Point Absorber

Figure 7 shows the relative position between the water level in the chamber and the cylindrical buoy during the two sea states. The first is Wave1 and the latter is Wave2. The analysis for Wave2 (the winter season) is carried out separately because the contribution of power from the solar panels is minimal, so 100% of the power would need to depend on the SB.

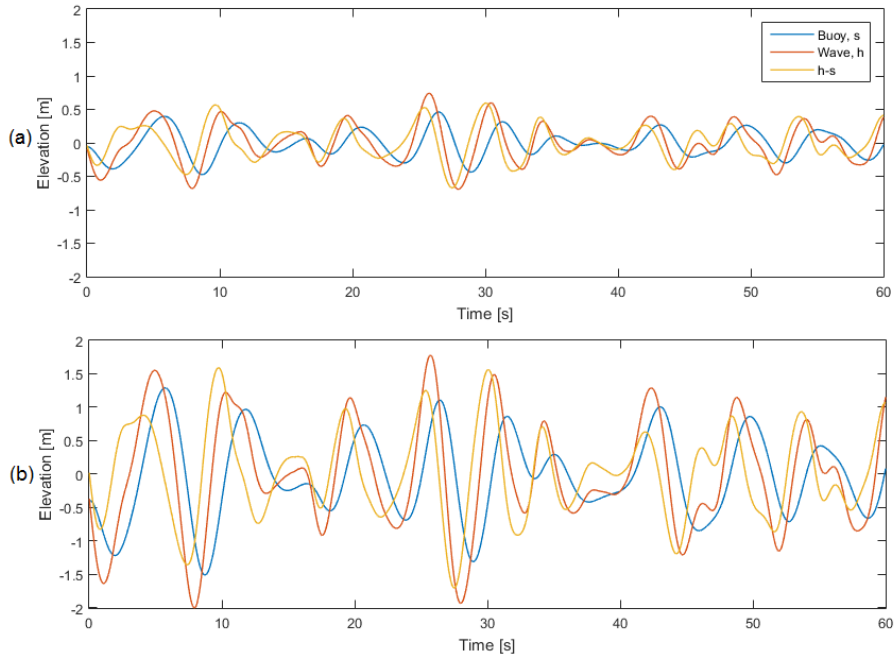

Figure 7. (**a**) Wave1; (**b**) Wave2. Blue indicates the vertical position of the cylindrical buoy. Red indicates the wave, h, inside the chamber. Yellow indicates the relative vertical position between wave, h, and cylindrical buoy, s.

Figure 8 shows the simulated result of the SB's vertical position relative to the cylindrical buoy. In Figure 8b, it can be seen that during winter the vertical position of the SB reaches the stroke limit of 1 m and will thus hit the end stops in the SB's chamber. However, it should be noted that Equations (11)–(13), used for the simulation, do not consider the presence of the end stop plates. This will affect the dynamics (and the performance) of the SB, but this is beyond the scope of the present study. For the Wave1 sea state, Figue 8a, the SB never reaches the maximum stroke.

The power extracted by the PTO depends on the damping coefficient, γ, and the SB's vertical velocity, $\dot{z}$, see Equation (14). The desired setting for γ can be realized by using a direct drive rotary generator or a linear generator. However, for this low power application and the small speed induced by the wave, a linear generator would be a better option [33]. Furthermore, by eliminating intermediate stages of energy conversion, such as hydraulic, pneumatic, or pumped water, a direct drive system is likely to reduce the mechanical failure modes as well as the need for maintenance [33]. The simulation of the average power extraction at two different damping coefficients, γ, for each of the two sea states can be seen in Figure 9. The power production is highest at $\gamma = 1.1$ kNs/m for the winter climate (Wave2) and at $\gamma = 660$ Ns/m for the most frequently occurring wave climate (Wave1). In the figure,

the damping coefficient for the device was set at $\gamma = 660$ Ns/m in order to prioritize maximum energy absorption at the most common sea states, resulting in an average power generation of 32.4 W. With this setting, the power absorption during the winter season is 153 W, which is beyond the required energy absorption.

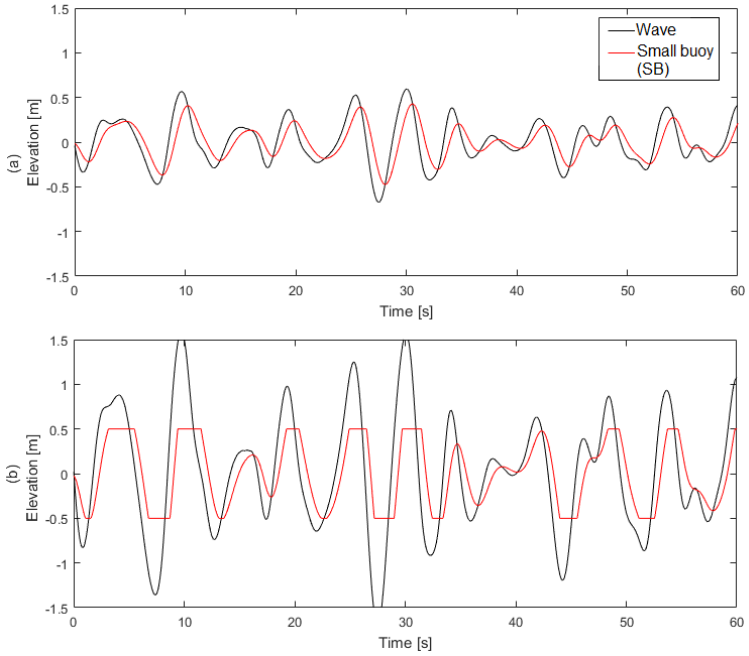

Figure 8. The vertical position of the small buoy (SB) in response to the relative position between buoy and wave inside the chamber. (**a**) Wave1; (**b**) Wave2. The SB clearly hits the end stops during Wave2.

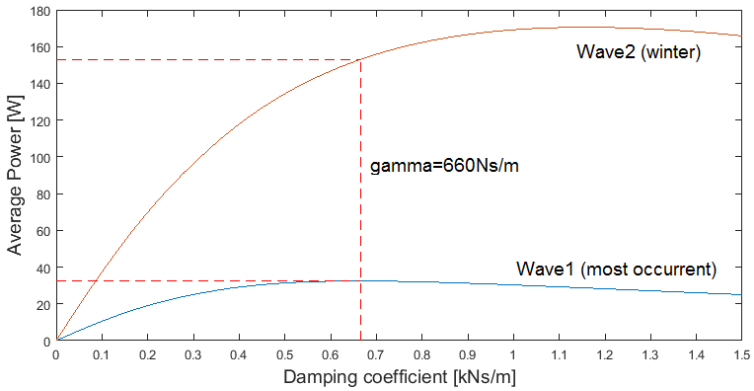

Figure 9. The two curves in the figure show the relation between different damping coefficients and average power for Wave1 and Wave2.

It should be noted that the buoy is assumed to move in heave only. This is a rather crude assumption, but the numerical model with only one degree of freedom has been validated with good agreement with experimental data [2], and experiments have also shown that the azimuthal inclination angle between the buoy and the generator at the seabed was less than 8 degrees [34], indicating that the surge and sway motions can be neglected. Nevertheless, it can be expected that the water column inside the buoy can have a more significant impact on the performance if more degrees of freedom are considered for the motion of the large buoy. Also, non-linear effects and viscous effects have been neglected in this paper. Whereas several studies have shown that linear potential flow theory can be used with acceptable accuracy to model certain aspects such as the motion of the buoy in operational

waves [2,35], to study a more realistic system and address viscous losses, full computational fluid dynamics (CFD) modeling would be required, but the computational cost of modeling such a large time series of waves needed for this study would be too high. Still, it should be remembered that the model is an approximation and that the computed power absorption is expected to be lower in reality.

The time series plot in Figure 10 shows the wave power available close to the Wave Hub (Lat: 50.375 and Lon: −5.625). The data is obtained from ECMWF re-analysis wave data from a two-year period (2015 and 2016) [36]. The temporal resolution is in 6 h averages. The red horizontal dashed line in the figure indicates the instantaneous power required by the small WEC to generate 37.7 W of electricity. The lowest potential in the two years of studied data occurred in June 2015 (marked with a red circle in Figure 10), with an average of 178 W over 6 h. This is translated to a 3.6 W absorption by the SB. However, because the solar irradiation is relatively high during this period of the year (March–September, see Table 4), the energy supplied for the compensator are mainly coming from solar PVs. The calculation for this PV output assumes that 70% of energy will be stored in the battery, while the rest of the energy consists of losses due to lower efficiency at high temperature and losses due to battery charging. Table 5 shows the parameters used to estimate the contribution of solar energy production to charge the battery. These parameters were based on CT50 Solar Marine solar panels [20] available on the market. In the worst case scenario that might occur when the energy from waves are minimal, as in June 2015, the number of solar panels needed to operate the compensator is at least 4. On the other hand, when the sea is completely calm, the full operation of the compensator is not needed, as the translator in the main WEC is also at rest. This approximation of required energy for the compensator operation was based on the maximum extension of 8 m. In reality, the characteristics of the tidal range at the Wave Hub was smaller at 6.6 m (in 2014). Considering this, in comparison with the calculations, around 17% percent less energy was required.

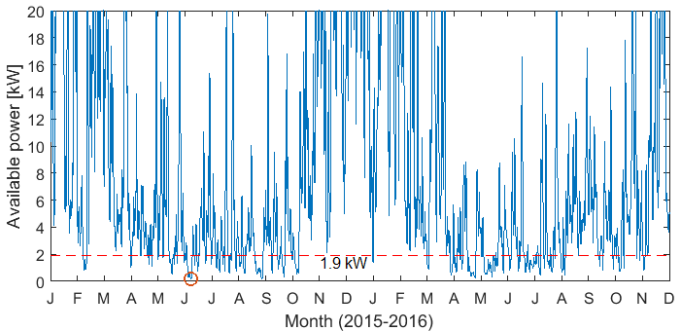

Figure 10. Wave power potential (in W) near Wave Hub (Lat: 50.375; Lon: −5.625) during 2015 and 2016. The red dashed line indicates the average power of the sea state that is needed for the small WEC to generate 37.7 W of electricity. The red circle indicates the least energetic sea state over the studied period.

Table 4. Average energy production (Wh/day) from a PV solar panel based on solar irradiation at the Wave Hub.

Month	Average Energy
Jan	29
Fab	52
Mar	104
Apr	168
May	189
Jun	222
Jul	193
Aug	155
Sep	129
Oct	70
Nov	37
Dis	23

Table 5. Parameter settings for energy estimation from solar PV panels (CT50 Solar Marine).

Parameter	Dimension
Nominal power for PV system	50 W
Inclination of module	0 deg.
Battery size	12 V, 100 Ah
Discharge cutoff limit (%)	40%

5. Conclusions

Based on the simulations, and with reasonable simplifications, the average power extractable for Wave1 (the most frequently occurring sea state) from a small OWC or a small heaving buoy, mounted inside a large WEC buoy, is 5.3 W and 32.4 W, respectively. A direct conclusion can be made that neither the OWC nor the heaving buoy is capable of providing enough energy to the compensator system by themselves. The compensator requires an average of 37.7 W in areas with 8 m and semidiurnal tides.

The position of the chamber inside the cylindrical buoy causes the surface elevation in the chamber to decrease compared to the incident wave. However, the phase shifts between the buoy motion, the incident wave, and the water column in the chamber results in a larger water column displacement—which benefits power production by the small buoy.

A hybrid system of solar energy and a small heaving point-absorbing WEC is considered to be the best option for supplying power to the sea-level compensation system. During the winter season, the solar energy is very low, but the energy contribution from the small buoy WEC is more than sufficient due to the more powerful sea states during the winter season. During the summer and based on the annually most commonly occurring sea state, Wave1, the small WEC alone does not produce enough energy, but the solar panels fully compensate for this.

Acknowledgments: The participation of Mohd Nasir Ayob is funded by Ministry of Education of Malaysia and Universiti Malaysia Perlis. Thanks go to the Swedish Energy Agency, Ångpanneföreningen, StandUP for Energy, Swedish Research Council grant 2015-04657 and the Carl Tryggers Foundation for their financial support.

Author Contributions: Mohd Nasir Ayob contributed extensively to designing and analyzing the simulation and to the writing of the manuscript. Valeria Castellucci contributed to the wave modeling. Malin Göteman and Jens Engström assisted in the WAMIT simulation. Joakim Widén assisted with solar irradiation estimation. Johan Abrahamsson provided knowledgeable discussion and suggestions. Rafael Waters conceived the idea, supervised, and gave final approval. All co-authors participated in writing the paper.

Conflicts of Interest: The authors declare no conflict of interest.

References

1. Sjökvist, L.; Krishna, R.; Rahm, M.; Castellucci, V.; Hagnestål, A.; Leijon, M. On the Optimization of Point Absorber Buoys. *J. Mar. Sci. Eng.* **2014**, *2*, 477–492.
2. Eriksson, M.; Waters, R.; Svensson, O.; Isberg, J.; Leijon, M. Wave power absorption: Experiments in open sea and simulation. *J. Appl. Phys.* **2007**, *102*, 084910, doi:10.1063/1.2801002.
3. Waters, R.; Stålberg, M.; Danielsson, O.; Svensson, O.; Gustafsson, S.; Strömstedt, E.; Eriksson, M.; Sundberg, J.; Leijon, M. Experimental results from sea trials of an offshore wave energy system. *Appl. Phys. Lett.* **2007**, *90*, 034105, doi:10.1063/1.2432168.
4. Tyrberg, S.; Svensson, O.; Kurupath, V.; Engstrom, J.; Stromstedt, E.; Leijon, M. Wave Buoy and Translator Motions—On-Site Measurements and Simulations. *IEEE J. Ocean. Eng.* **2011**, *36*, 377–385.
5. Castellucci, V.; Abrahamsson, J.; Svensson, O.; Waters, R. Algorithm for the calculation of the translator position in permanent magnet linear generators. *J. Renew. Sustain. Energy* **2014**, *6*, 063102, doi:10.1063/1.4900553.
6. Engström, J.; Eriksson, M.; Isberg, J.; Leijon, M. Wave energy converter with enhanced amplitude response at frequencies coinciding with Swedish west coast sea states by use of a supplementary submerged body. *J. Appl. Phys.* **2009**, *106*, 064512, doi:10.1063/1.3233656.
7. Engström, J.; Kurupath, V.; Isberg, J.; Leijon, M. A resonant two body system for a point absorbing wave energy converter with direct-driven linear generator. *J. Appl. Phys.* **2011**, *110*, 124904, doi:10.1063/1.3664855.
8. Castellucci, V.; Waters, R.; Eriksson, M.; Leijon, M. Tidal effect compensation system for point absorbing wave energy converters. *Renew. Energy* **2013**, *51*, 247–254.
9. Ayob, M.N.; Castellucci, V.; Terzi, M.; Waters, R. Tidal Effect Compensation System Design for High Range Sea Level Variations. In Proceedings of the 11th European Wave and Tidal Energy Conference (EWTEC), Nantes, France, 6–11 September 2015.
10. Wave Hub Test Site. Available online: https://www.wavehub.co.uk/wave-hub-sit (accessed on 21 February 2017).
11. Van Nieuwkoop, J.C.; Smith, H.C.; Smith, G.H.; Johanning, L. Wave resource assessment along the Cornish coast (UK) from a 23-year hindcast dataset validated against buoy measurements. *Renew. Energy* **2013**, *58*, 1–14.
12. British Oceanographic Data Centre. Available online: https://www.bodc.ac.uk (accessed on 11 May 2016).
13. Castellucci, V.; Eriksson, M.; Waters, R. Impact of Tidal Level Variations on Wave Energy Absorption at Wave Hub. *Energies* **2016**, *9*, 843, doi:10.3390/en9100843.
14. Castellucci, V.; Abrahamsson, J.; Kamf, T.; Waters, R. Nearshore Tests of the Tidal Compensation System for Point-Absorbing Wave Energy Converters. *Energies* **2015**, *8*, 3272–3291.
15. Masuda, Y. *Hydrodynamics of Ocean Wave-Energy Utilization*; Springer: Berlin/Heidelberg, Germany, 1986; pp. 445–452.
16. Henriques, J.C.; Portillo, J.C.; Gato, L.M.; Gomes, R.P.; Ferreira, D.N.; Falcão, A.F. Design of oscillating-water-column wave energy converters with an application to self-powered sensor buoys. *Energy* **2016**, *112*, 852–867.
17. Chiba, S.; Waki, M.; Wada, T.; Hirakawa, Y.; Masuda, K.; Ikoma, T. Consistent ocean wave energy harvesting using electroactive polymer (dielectric elastomer) artificial muscle generators. *Appl. Energy* **2013**, *104*, 497–502.
18. Bonfiglioli. Available online: http://www.bonfiglioli.com (accessed on 21 February 2017).
19. Intorq. Available online: http://www.intorq.com (accessed on 21 February 2017).
20. For Info on Solar Panel. Available online: https://www.elfa.se (accessed on 21 February 2017).
21. Regional Coastal Monitoring Programmes. Available online: http://www.channelcoast.org (accessed on 11 December 2017).
22. Chakrabarti, S.K. *Hydrodynamics of Offshore Structures*; WIT Press: Southampton, UK, 1987.
23. Huld, T.; Müller, R.; Gambardella, A. A new solar radiation database for estimating PV performance in Europe and Africa. *Sol. Energy* **2012**, *86*, 1803–1815.
24. Sarmento, A. Wave flume experiments on two-dimensional oscillating water column wave energy devices. *Exp. Fluids* **1992**, *12*, 286–292.
25. Evans, D.V.; Porter, R. Efficient Calculation of Hydrodynamic Properties of OWC-Type Devices. *J. Offshore Mech. Arct. Eng.* **1997**, *119*, 210–218.

26. Morris-Thomas, M.T.; Irvin, R.J.; Thiagarajan, K.P. An Investigation Into the Hydrodynamic Efficiency of an Oscillating Water Column. *J. Offshore Mech. Arct. Eng.* **2007**, *129*, 273–278.
27. Ram, K.; Faizal, M.; Rafiuddin Ahmed, M.; Lee, Y.H. Experimental studies on the flow characteristics in an oscillating water column device. *J. Mech. Sci. Technol.* **2010**, *24*, 2043–2050.
28. Bayoumi, S.; Incecik, A.; El-Gamal, H. Dynamic modelling of Spar-Buoy oscillating water column wave energy converter. *Ships Offshore Struct.* **2015**, *10*, 601–608.
29. Garrido, A.J.; Otaola, E.; Garrido, I.; Lekube, J.; Maseda, F.J.; Liria, P.; Mader, J. Mathematical Modeling of Oscillating Water Columns Wave-Structure Interaction in Ocean Energy Plants. *Math. Probl. Eng.* **2015**, *2015*, 1–11.
30. Da Rosa, A. Wind Energy. In *Fundamentals of Renewable Energy Processes*; Bodc, Ed.; Elsevier: Amsterdam, The Netherlands, 2013; pp. 685–763.
31. Stoker, J.J. Basic Hydrodynamics. In *Water Waves*; John Wiley & Sons, Inc.: Hoboken, NJ, USA, 2011; pp. 1–18.
32. Ivanova, I.; Bernhoff, H.; Ågren, O.; Leijon, M. Simulated generator for wave energy extraction in deep water. *Ocean Eng.* **2005**, *32*, 1664–1678.
33. Rhinefrank, K.; Schacher, A.; Prudell, J.; Brekken, T.K.A.; Stillinger, C.; Yen, J.Z.; Ernst, S.G.; von Jouanne, A.; Amon, E.; Paasch, R.; et al. Comparison of Direct-Drive Power Takeoff Systems for Ocean Wave Energy Applications. *IEEE J. Ocean. Eng.* **2012**, *37*, 35–44.
34. Savin, A.; Svensson, O.; Leijon, M. Azimuth-inclination angles and snatch load on a tight mooring system. *Ocean Eng.* **2012**, *40*, 40–49.
35. Sjökvist, L.; Wu, J.; Ransley, E.; Engström, J.; Eriksson, M.; Göteman, M. Numerical models for the motion and forces of point-absorbing wave energy converters in extreme waves. *Ocean Eng.* **2017**, *145*, 1–14.
36. European Centre for Medium-Range Weather Forecasts. Available online: http://apps.ecmwf.int/datasets/data/interim-full-daily (accessed on 18 March 2017).